Structural principles to steer the selectivity of the electrocatalytic reduction of aliphatic ketones on platinum

Bondü, C.J.; Calle Vallejo, F.; Costa Figueiredo, M.; Koper, M.T.M.

Structural Principles to Steer the Selectivity of the Electrocatalytic Reduction of Aliphatic Ketones on Platinum

Christoph J. Bondue [a], Federico Calle-Vallejo [b], Marta C. Figueiredo [a], Marc T. M. Koper [a,]

[a] Leiden Institute of Chemistry, Leiden University, P.O. Box 9502, 2300 RA Leiden, The Netherlands.

[b] Departament de Ciència de Materials i Química Fisica & Institut de Química Teòrica i Computacional (IQTCUB), Universitat de Barcelona, Martí i Franquès 1, 08028 Barcelona, Spain.

Keywords: Hydrogenation, hydrolysis, ketone, electrocatalysis, single crystal electrode.

TOC entry

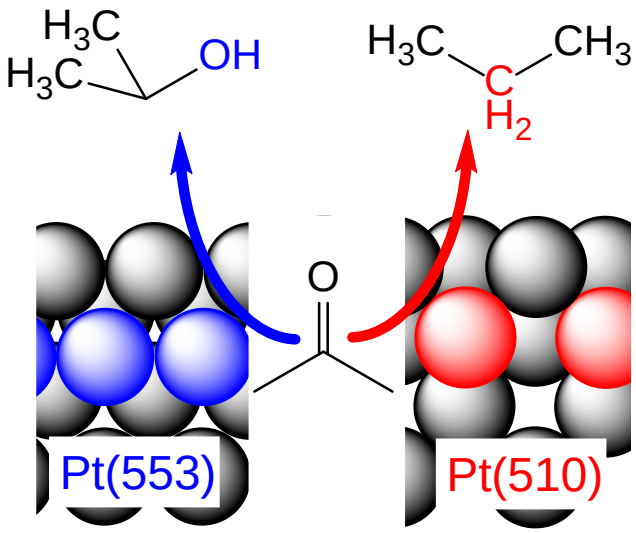

ABSTRACT

Due to a general shift of the resource basis, chemical industry is charged with the task of finding ways to transform ketones to value-added products. A viable route to do so is the electrochemical hydrogenation of the carbonyl functional group. Here we report a study on acetone reduction at platinum single-crystal electrodes using online electrochemical mass spectroscopy, in situ FTIR spectroscopy and DFT calculations. Acetone reduction at platinum displays a remarkable structural sensitivity: not only the activity but also the product distribution depends on the surface crystallographic orientation. At Pt(111) neither adsorption nor hydrogenation occur. A decomposition reaction deactivating the electrode happens at Pt(100). Acetone reduction proceeds at (110) steps: while Pt[(n-1)(111)x(110)] electrodes produce 2-propanol, Pt[(n+1)(100)x(110)] electrodes produce propane. Using DFT calculations, we build a selectivity map to explain the intricacies of the acetone reduction on platinum. Finally, we extend our conclusions to the reduction of higher aliphatic ketones.

Pyrolysis of lignin-rich waste materials and biomass to bio-oils has the potential to become a new, valuable source of aromatic platform chemicals[1]. However, bio-oils consist of carboxylic acids, ketones and aldehydes that need further refinement[2-4]. Therefore, studies on the electrochemical hydrogenation of carbonyl compounds such as acetophenone[5], benzaldehyde [6,7], 5-hydroxymethyllfurfural[8-10], or ethyl pyruvate[11,12] have received renewed attention, as they might give valuable insight into the electrorefinement of biomass. The electrochemistry of the ethyl pyruvate is also interesting because it is the standard substrate of the Orito reaction by which α-keto esters can be enantioselectively hydrogenated using heterogeneous catalysis[13]. However, each of these carbonyl compounds features a second functional group that is also susceptible to hydrogenation. For instance, the phenyl ring of acetophenone behaves similarly to benzene, which has a rich and rather complex electrochemistry of its own[14].

To provide fundamental knowledge on the electrochemistry of carbonyl functional groups, here we study the electrochemical reduction of acetone as a model system for the electroreduction of carbonyl compounds. As acetone is the simplest ketone, its reduction is not convoluted by the presence of additional functional groups or by the formation of acetals. It was shown previously that acetone can be reduced electrochemically at polycrystalline platinum electrodes[15-19] to both propane and 2-propanol[16,17]. To the best of our knowledge, single crystal studies on the electrochemical hydrogenation of acetone have never been reported. However, Hazzazi *et al*. showed that ethyl pyruvate adsorbs preferentially at (110) steps at Pt electrodes and, via CO formation, at Pt(100) terraces[11]. This suggests a strong influence of the surface structure on the electrochemistry of ketones.

In this study, we employ single crystal platinum electrochemistry in combination with in situ and online techniques (infrared spectroscopy FTIR and online electrochemical mass spectroscopy, OLEMS) to show that activity, selectivity and the extent of catalytic poisoning of acetone electroreduction are highly sensitive to the platinum surface structure. Using DFT calculations, we

propose detailed pathways for the electrocatalytic reduction of acetone to 2-propanol and propane, and show that the product selectivity is driven by the coordination of the active sites.

RESULTS

Acetone Reduction at Single Crystal Platinum Electrodes

Figure 1A shows the CVs at stepped Pt(111)-type single crystal electrodes in an electrolyte of 0.1 M H_2SO_4 containing 0.1 M acetone. At all stepped electrodes a peak due to hydrogen desorption from (110) step sites is observed in the positive going sweep at approximately 0.12 V. In the blank electrolyte the corresponding reduction peak appears in the negative going scan at the same potential. Such a peak is missing in the presence of acetone (c.f. Supplementary Figures 1 to 6) and indicates strong adsorption of acetone at (110) step sites (the interaction between (110)-step sites and acetone is rather strong as further explained by Supplementary Figure 7 and Supplementary Note 2). Hydrogen adsorption is only possible once acetone is fully removed from the surface. No acetone adsorption is observed at Pt(111) terraces as the presence of acetone does not suppress the sulfate spike or the H-upd peak at Pt(111) (c.f. Supplementary Figure 1 and Supplementary Note 1).

In the presence of acetone, a peak at 0.05 V appears in the negative going sweep at Pt(554), Pt(553), Pt(331) and Pt(110), indicating the reduction of the ketone. At an electrode with long terraces such as Pt(15,15,14) only a faint shoulder is observed, while any indication for acetone reduction is missing at Pt(111). Considering that acetone does not adsorb on (111) terraces, the inactivity of Pt(111) is not surprising. Figure 1B illustrates that the activity for acetone reduction only stems from the (110) step sites: the current density at 0.05 V increases linearly as the theoretical step density increases from 0 (i.e. Pt(111)) to 0.23 (i.e. Pt(553)). However, for step densities larger than 0.23 the current density plateaus (the same behavior is observed in Supplementary Figure 8 where the current density is plotted versus the experimentally determined surface step density as determined in Supplementary Note 3). In principle, this means that the activity of the individual (110)

steps decreases for high densities. In other words, the nominal turnover frequency per step site is lower at Pt(110) compared to Pt(553).

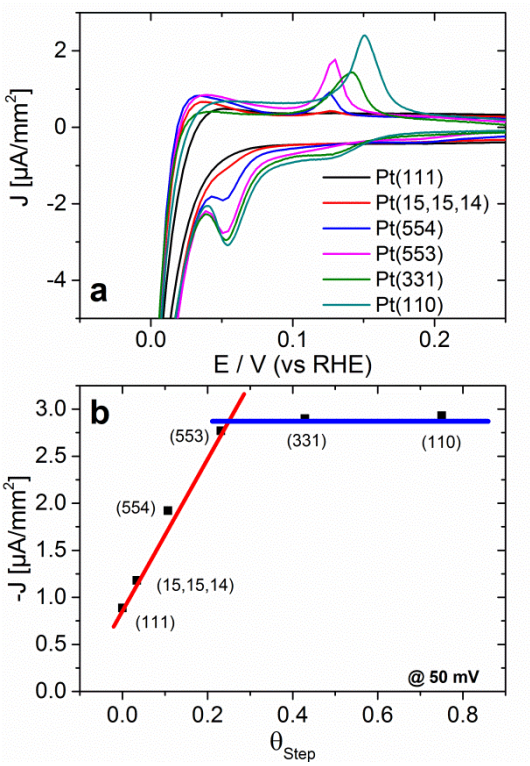

Figure 1. Influence of the theoretical step density of Pt[(n-1)(111)x(110)] electrodes on acetone reduction. A) CVs at various stepped Pt(111) electrodes (Pt[(n-1)(111)x(110)]) in 0.1 M H_2SO_4 containing 0.1 M acetone. B) Current density at 0.05 V plotted as a function the theoretical of step density (no (1x2)-reconstruction is considered). Full potential sweeps for each electrode both in the blank electrolyte and in acetone containing electrolyte appear in Supplementary Figures 1-6 in. A plot of the current density versus the charge of the hydrogen desorption peak (as a measure for the real step density) can be found in Figure S8 in the SI.

As long as the number of adsorption sites is the only limiting factor, the current density follows the step density linearly. However, steric hindrance or any other step-step interaction between adsorbed species may limit the maximal achievable surface concentration. This situation appears to be achieved at Pt(553). Increasing the step density further does not result in a higher surface concentration. As will be shown later in Figures 6-7, individual step sites on Pt(110) are

predicted to be more active than those of Pt(553) because their generalized coordination number ($\overline{CN}$ [20], see page S6 in the SI) is close to optimal, but experiments suggest that they participate less frequently in acetone hydrogenation. There appears to be a compensation effect between the density of active sites and their intrinsic activity. A similar effect has been invoked for the hydrogenation of benzene at stepped Pt(111) terraces[21] and for oxygen reduction on stepped Pt(111)[22].

Hydrogen evolution and acetone reduction are the only reactions occurring at stepped Pt(n(111)x(110)) electrodes. That is, there is no side reaction that leads to the poisoning of the electrode. As discussed in Supplementary Note 4 this is can be derived from Supplementary Figure 9A in which a Pt(553) electrode has been cycled for a prolonged period of time without any effect on the shape of the CV. This is in contrast to other aldehydes (i.e. acetaldehyde) which interact with platinum surfaces by cleavage of the C-C bond, resulting in the accumulation of CH_x-species and carbon monoxide on the electrode[23].

Let us now analyze the effect of changing the terrace symmetry from (111) to (100) while keeping the same type of steps. Figure 2A shows the CVs obtained in an electrolyte of 0.1 M H_2SO_4 containing 0.1 M acetone at stepped Pt(100) electrodes. A shoulder prior to hydrogen evolution appears in the CV of Pt(10,1,0) and, more prominently, of Pt(510) in the presence of acetone. The shoulder indicates ketone reduction, and is missing in the CV of pristine Pt(100). Similar to stepped Pt(111) electrodes, the activity of stepped Pt(100) electrodes increases with step density. The most likely interpretation for this observation is that the electrochemical hydrogenation takes place at (110) step sites. Computational studies suggest that the activity for acetone reduction at stepped Pt(100) electrodes stems from step sites (see below), while the terraces are inactive for acetone reduction. In addition, the discussion of Supplementary Figures 10 to 12 in Supplementary Note 5 provides further arguments why also the CV data suggest that the active surface sites for acetone reduction are the step sites.

Aside from acetone reduction, a reaction occurs at stepped Pt(100) electrodes that leads ultimately to poisoning: Supplementary Figure 9B shows that Pt(510) loses all its activity for acetone reduction after the third cycle. In order to identify the active surface site for the poisoning reaction we have conducted the potential opening experiment in Figure 2B. Each cycle in Figure 2B is the first potential scan recorded at a freshly prepared Pt(100) electrode in an electrolyte of 0.1 M H_2SO_4 containing 0.1 M acetone. As long as the lower potential window remains above 0.7 V, only capacitive currents are observed in the CV. However, when the lower potential limit goes below 0.7 V an oxidation current appears in the negative-going scan, with a corresponding oxidation current in the potential region between 0.7 V and 0.85 V in the following positive-going scan. These results suggest that acetone is oxidized at (100) terraces at potentials below 0.7 V. This oxidation is incomplete, since further oxidation takes place in the potential region between 0.7 V and 0.85 V.

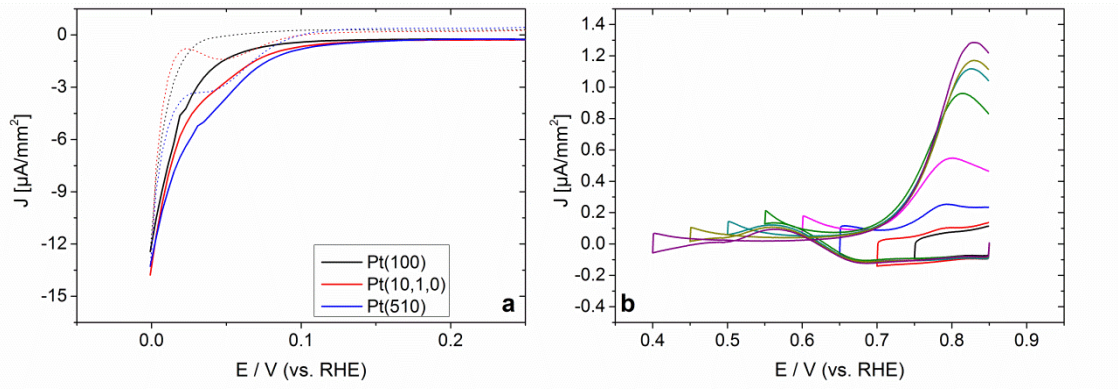

Figure2. Processes at Pt[(n+1)(100)x(110)] electrodes. A) CVs at stepped Pt(100) electrodes (Pt[(n+1)(100)x(110)]) in 0.1 M H_2SO_4 containing 0.1 M acetone. Solid lines: negative going sweep; dotted lines: positive going sweep. B) Potential opening experiment at a Pt(100) electrode. A full potential sweep for each electrode can be found in Figures S10 to S12 in the SI. Sweep rate: 0.05 V/s; Potential limits: 0 V to 0.85 V.

When we accumulate products of incomplete acetone oxidation by exposing a Pt(510) electrode for 2 minutes to an acetone containing electrolyte at 0.45 V, the electrode loses its ability to reduce acetone (c.f. Supplementary Figure 13 and Supplementary Note 6). However, exposing the electrode for 2 minutes to the same solution at 0.85 V, where acetone does not undergo a reaction, does not impair acetone reduction in the following negative going sweep. This suggests that the

oxidation process observed at Pt(100) in the potential range between 0.7 V and 0.45 V causes the poisoning of stepped Pt(100) electrode. That is, it suggests that the Pt(100) terraces are the active surfaces sites for electrode poisoning. Although we do not study the nature of the poisoning reaction in detail, it is interesting to note its sensitivity to the crystallographic orientation of the electrode.

Product Distribution of Acetone Reduction

To demonstrate the influence of surface orientation on product distribution, Figure 3 shows OLEMS results obtained at Pt(553) and Pt(510) during potential steps into the potential window of acetone reduction. After each step, an intense signal in the ionic current for mass 2 is observed (Figure 3B and 3E) corresponding to hydrogen evolution. Since the signal intensity at both crystals is roughly the same, we can infer that the sensitivity for the two experimental setups is comparable. Parallel to hydrogen evolution signals in the ionic currents for masses 27, 29 and 44 with an intensity ratio of $I_{29} : I_{27} : I_{44}$ is 100 : 43 : 24 are observed in the experiments conducted at Pt(510) (Figure 3C). Only faint signals for the same masses are observed for Pt(553) (Figure 3F).

The observed masses and intensity ratio correspond to the fragmentation pattern of propane, and indicates significant acetone reduction to propane on Pt(510). Since only a faint signal for propane formation is observed during acetone reduction at Pt(553), we derive that the hydrocarbon is only a minor product of acetone reduction. Hence, the dominant product of acetone reduction at Pt(553) electrodes should be 2-propanol. Note that alcohols are difficult to detect by means of OLEMS, because they do not pass readily from the aqueous phase into the vacuum of the mass spectrometer.

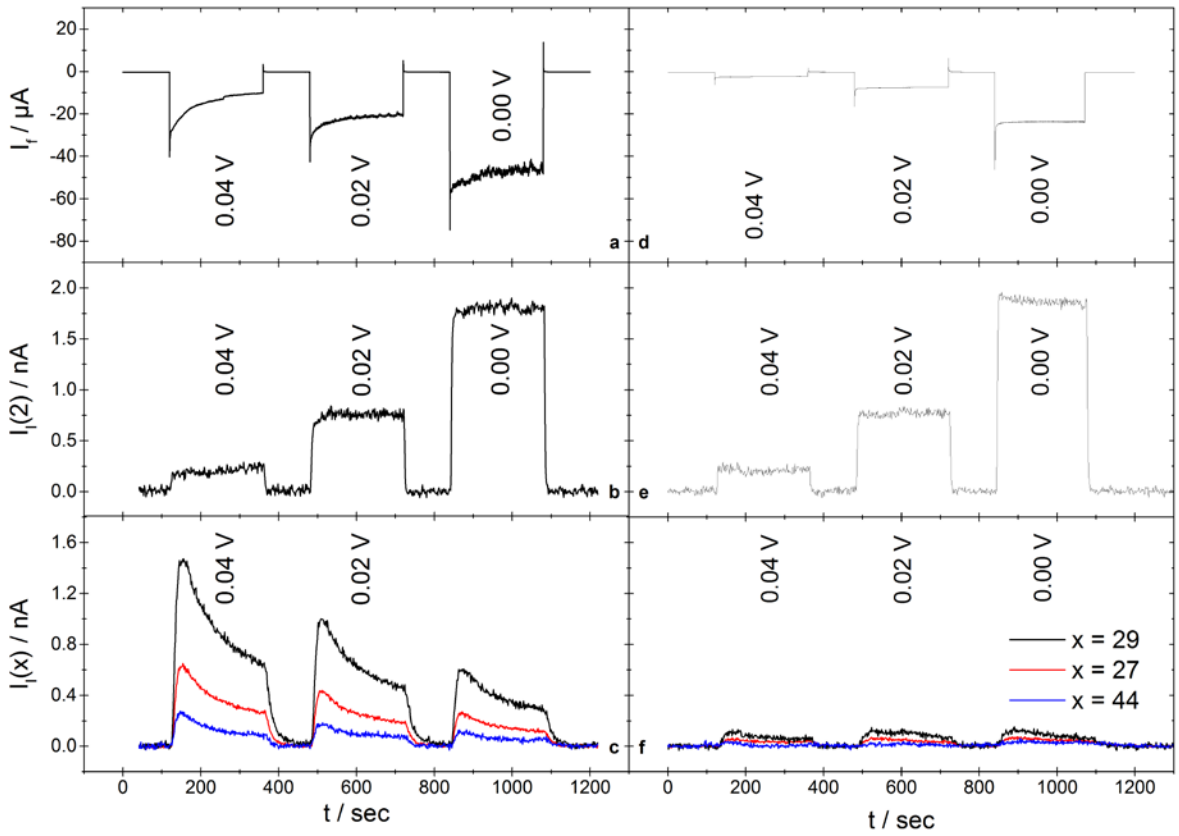

Figure 3. Structure sensitivity of propane formation upon acetone reduction. OLEMS results obtained at Pt(510) (left) and Pt(553) (right). The step potential program was 0.85 V, 0.04 V, 0.85 V, 0.02 V, 0.85 V, 0 V and 0.85 V. A and D: faradaic current; B and E: Ionic current for mass 2; C and F: ionic current for mass 29 (black), 27 (red) and 44 (blue). Electrolyte: 0.1 MH_2SO_4 containing 0.1 M acetone.

The FTIR spectra in Figure 4 confirm the assertion that acetone is reduced to 2-propanol at Pt[(n-1)(111)x(110)] electrodes. After a potential step to 0.05 V at Pt(110), two bands at 2971 cm^{-1} and 2877 cm^{-1} appear. These bands correspond to the asymmetric and symmetric stretching vibrations of the methyl groups of 2-propanol at $\nu(CH_3)_{as}$ = 2971 cm^{-1} and at $\nu(CH_3)_s$ = 2888 cm^{-1} [24]. On the other hand, propane has only a single band at 2940 cm^{-1} due to both $\nu(CH_3)_{as}$ and $\nu(CH_3)_s$ [25]. The appearance of two bands therefore strongly indicates that acetone is reduced only to 2-propanol at Pt(110). If propane was formed, a third band would be expected in Figure 4. Although perfect

selectivity cannot be proven with the employed techniques, it can be asserted that acetone is reduced to 2-propanol with good selectivity at Pt[(n-1)(111)x(110)] electrodes.

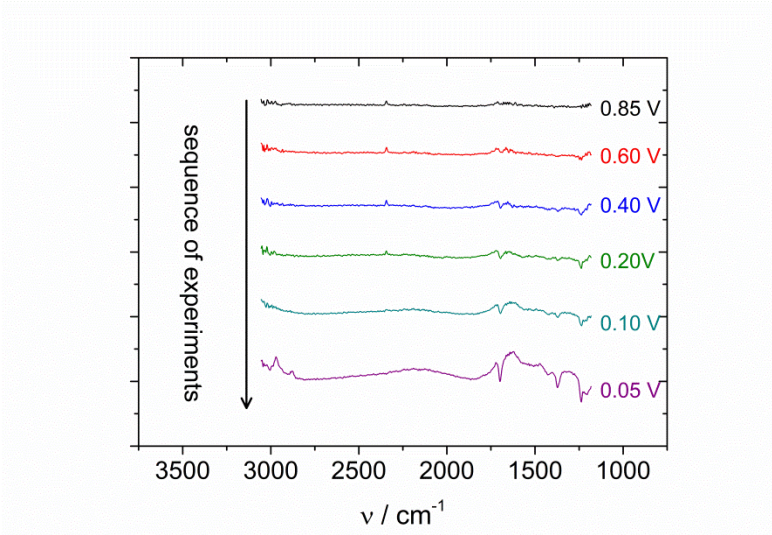

Figure 4. FTIR spectra obtained at Pt(110) and at the indicated potentials in an electrolyte of 0.1 M H_2SO_4 containing 0.1 M acetone.

Aside from the positive bands at 2971 cm^{-1} and 2877 cm^{-1}, there are three negative bands at 1697 cm^{-1}, 1370 cm^{-1} and 1237 cm^{-1} in Figure 4. These bands correspond to the symmetric stretching vibration of the C-O bond ($\nu(C\text{-}O)_s$ = 1710 cm^{-1}), the symmetric deformation vibration of the methyl groups ($\delta(Me)_{as}$ = 1361 cm^{-1}) and the asymmetric stretching vibration of the carbon skeleton ($\nu(Me\text{-}C\text{-}Me)_{as}$ = 1220 cm^{-1}) of free acetone[26 27]. These bands suggest the depletion of acetone from the thin layer between electrode and prism. This happens already at potentials more positive than 0.05 V and before the formation of 2-propanol indicates the electrochemical consumption of acetone. Given our conclusion that acetone starts to adsorb at Pt(553) in the potential range between 0.4 V and 0.6 V (c.f. Figure S7), it is likely that the negative bands are due to the adsorption of acetone.

The FTIR-Spectra in Figure 4 do not feature any positive bands that could be assigned to adsorbed acetone. However, the large background due to water and acetone in the gap between prism and electrode makes it difficult to observe weak bands in FTIR spectra. In the SI, we provide

Raman spectra that show that acetone adsorbed in a Raman active mode experience a weakening of the C-O binding strength (Supplementary Figure 14 in Supplementary Note 7).

Computational Modelling of Acetone Reduction

To gain insight into the intriguing structure-sensitive selectivity of acetone reduction, we now resort to DFT calculations. We have modelled acetone reduction on six sites at Pt surfaces (see the structures and active sites in Supplementary Figure 16; Supplementary Note 8) through the reaction networks shown in Supplementary Figure 15. After modelling all the possible pathways in Supplementary Figure 15 (including those starting with propenol, the enol tautomer of acetone), we conclude that the most favorable pathways for acetone reduction to 2-propanol and propane, namely those with the lowest overpotential, are those in Figure 5. Both pathways proceed via acetone molecular adsorption and subsequent hydrogenation to $*CH_3COHCH_3$. If the carbon atom bound to the surface of this intermediate is hydrogenated, 2-propanol is formed. Conversely, if the C-O bond is cleaved, propane and water are produced. Thus, there are two key factors for acetone reduction: first, whether acetone adsorbs or not determines the activity of the catalyst. Second, the relative ease of protonation or C-O bond scission of $*CH_3COHCH_3$ determines the selectivity of the reaction.

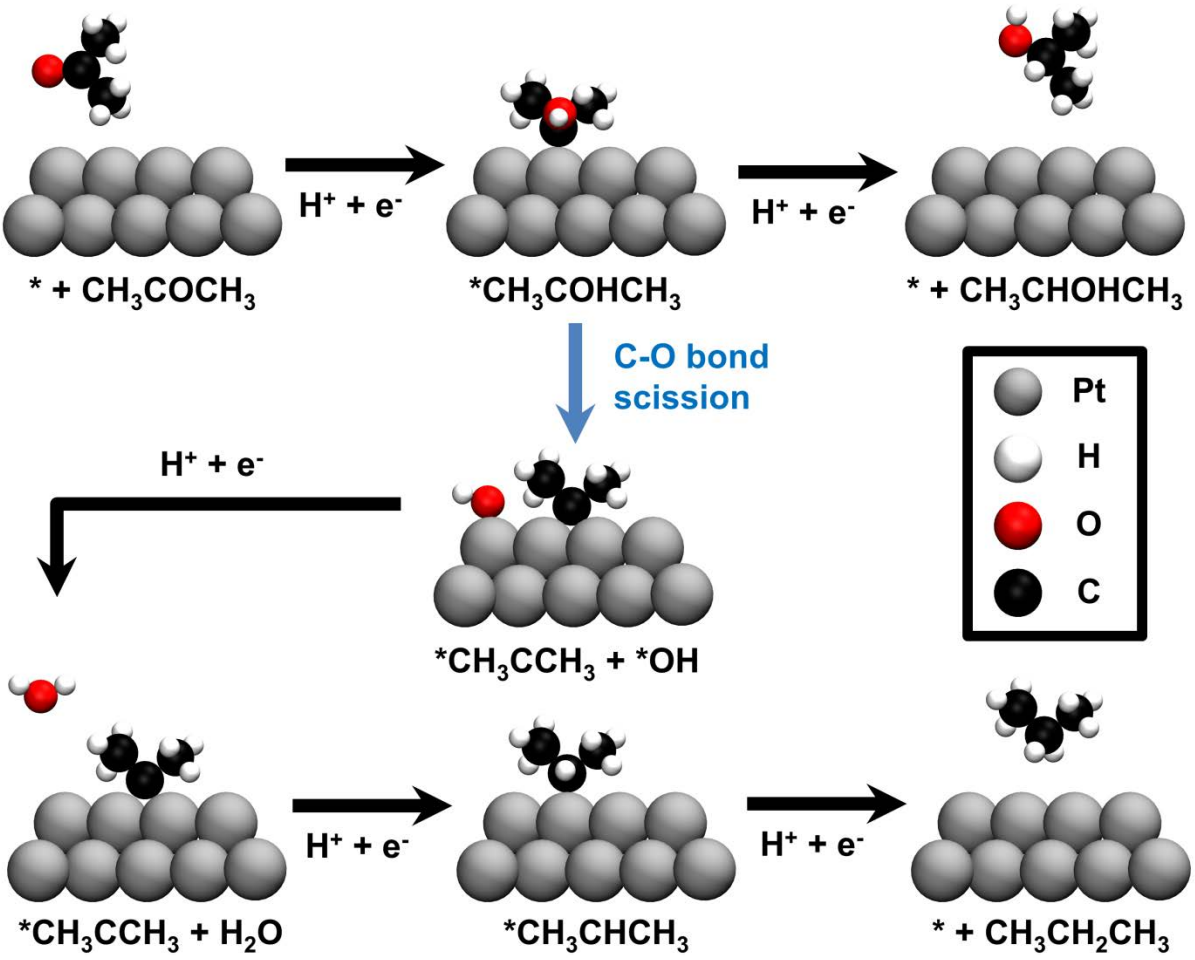

Figure 5. Most favorable reaction pathways for acetone reduction to 2-propanol and propane at Pt electrodes. The entire reaction networks from which they were derived appear in Supplementary Figure 15.

First, let us focus on the activity trends among Pt sites. In Figure 6 we provide separate coordination-activity plots for 2-propanol and propane production modelled following the pathways in Figure 5. For 2-propanol production the most active surface is Pt(110). Since only two electrons are transferred in this reaction, the top of the volcano and the equilibrium potential coincide in Figure 6A[28]. The orange line in the plot (weak binding sites) corresponds to acetone hydrogenation to $*CH_3COHCH_3$ being the potential-determining step. The green line (strong binding sites) corresponds to the hydrogenation of $*CH_3COHCH_3$ to produce 2-propanol being the potential-determining step. The inset shows the correlation between $\overline{CN}$ and the adsorption energies of acetone. The red dashed line at $\overline{CN} \approx 6.0$ corresponds to the limit of exothermic acetone adsorption on Pt facets

(Supplementary Figure 18B in Supplementary Note 8 shows that for $\overline{CN} \leq 5.8$ acetone adsorption energies are more favorable than those of *H).

Figure 6B shows that Pt(510) is predicted to be the most active surface under study for propane production. The orange line (weak binding) in the plot corresponds again to acetone hydrogenation. The blue line (strong binding) represents the hydrogenation of $*CH_3CCH_3$ to $*CH_3CHCH_3$. The inset shows that for $\overline{CN} < 6.2$ (purple line in the main panel), $*CH_3COHCH_3 + * \rightarrow *CH_3CCH_3 + *OH$ is thermodynamically favorable, which is necessary to shift the selectivity toward propane production.

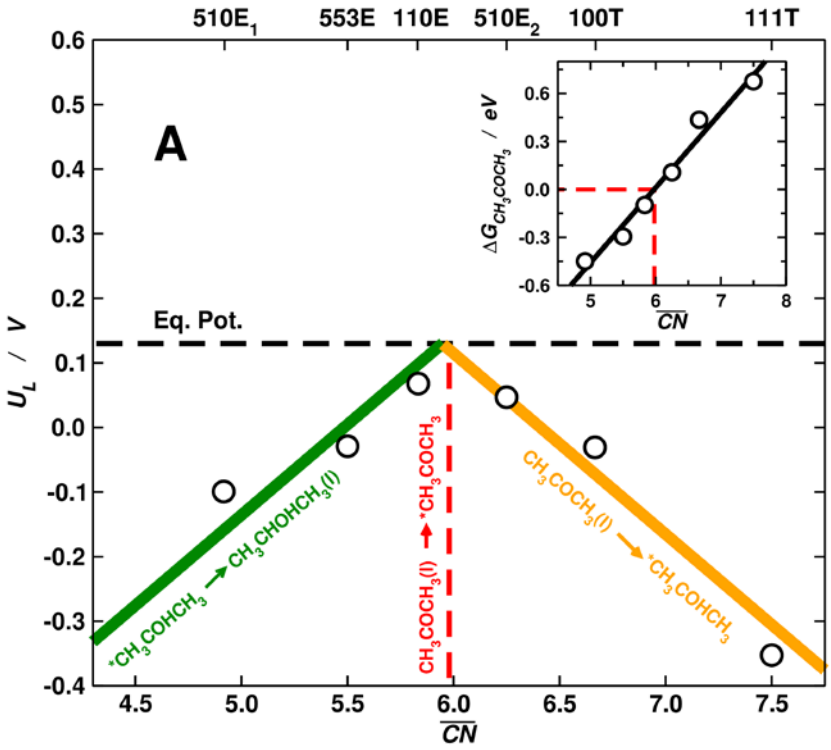

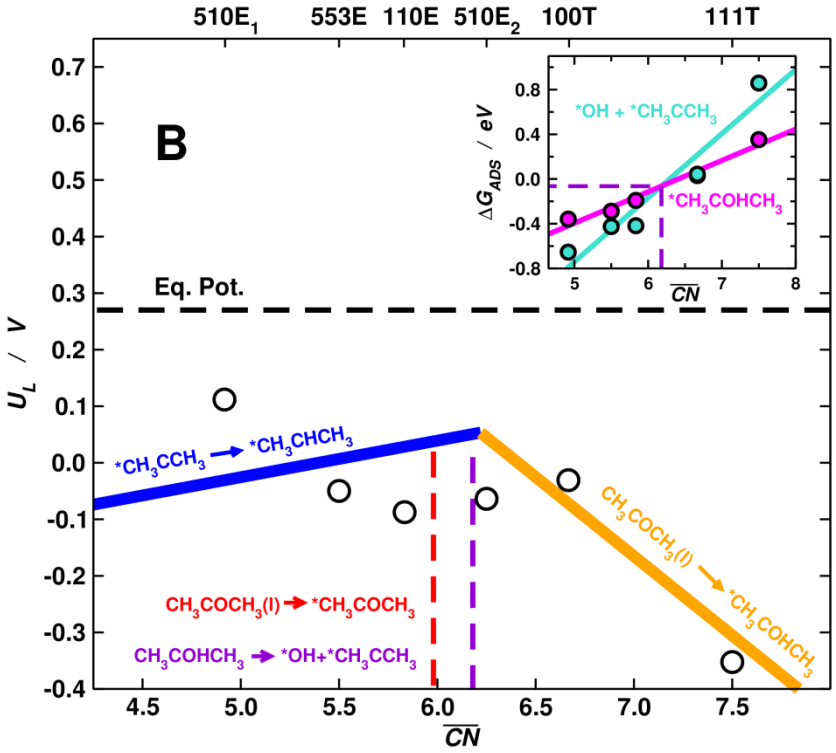

Figure 6. Coordination-activity plots for acetone reduction. reduction to (A) 2-propanol, and (B) propane. Six different Pt surface sites are studied, see the top x-axis and Supplementary Figure 16. The most favorable onset potentials (U_L) are reported for each site. The dots are calculated data points from the DFT simulations. The orange, green and blue lines come from Supplementary Figure 18A and result from the correlations between generalized coordination numbers and adsorption energies. The mean absolute errors between the fits and the calculated data points are in all cases smaller than 0.10 eV. The black dashed lines correspond to the equilibrium potentials. The red line comes from the inset in (A) and separates sites with/without (left/right) exothermic acetone adsorption. The purple line comes from the inset in (B) and separates sites for which $*CH_3COHCH_3 + * \rightarrow *CH_3CCH_3 + *OH$ is exothermic/endothermic (left/right).

Furthermore, Figure 5 shows that the pathway of acetone reduction bifurcates before 2-propanol is formed. This suggests that once the alcohol is formed no further reduction is possible. Indeed, we arrive at the same conclusions experimentally: Supplementary Figure 19 and the related discussion in Supplementary Note 9 shows that 2-propanol cannot be reduced at the Pt(510) electrode under the same conditions under which acetone is reduced to propane.

It is useful to determine whether and how coordination influences the pathway bifurcation. In Figure 7 we have overlapped Figures 6A and B together with the H_2 evolution trends from ref.[29] to provide a selectivity map that predicts the most favorable product of acetone reduction and its onset potential based on the geometry of the Pt active sites. Essentially, we detect three regions:

1) For large coordination number ($\overline{CN} > 6.6$, red lines in Figure 7), *H adsorption and H_2 evolution are most favorable (see also Supplementary Figure 18 B), so the sites are inactive for acetone reduction. This is the case for the terrace sites at Pt(111) and Pt(100).

2) For intermediate coordination number, the orange line in Figure 7 ($6.0 < \overline{CN} < 6.6$) marks the region in which 2-propanol formation is more favorable than H_2 evolution, but acetone molecular adsorption is endothermic. On sites with coordination in the range $5.5 < \overline{CN} < 6.0$ (green line in Figure 7), acetone adsorption becomes exothermic and more favorable than that of *H (Supplementary Figure 18B), and $*CH_3COHCH_3$ hydrogenation is more favorable than the scission of the C-O bond, so that 2-propanol predominates in the product distribution. This is the case of for Pt(110) and for the step sites in Pt(553).

3) For low coordination number ($\overline{CN} < 5.5$, blue line), the cleavage of the C-O bond in $*CH_3COHCH_3$ is rather favorable, so that propane is the preferred product. This is the case for the undercoordinated step sites on Pt(510) ($510E_1$ sites in Figure 7).

The slopes of the lines in Figure 7 come from Figure 6 and give an account of the structural dependence of the potential-determining steps of each reaction pathway. The orange and green lines are steeper than the blue one because in the former two the reaction energy involves only a single adsorbed intermediate. Conversely, the blue line involves two adsorbed species (one as a reactant, another as a product), which leads to a small slope because of the similarity between the adsorbed species. This is illustrated in Supplementary Figure 18, where it is also shown that the mean absolute errors between the calculated data points and the fits are below 0.10 eV in all cases. The

red lines for H_2 evolution have a small slope because the variations in hydrogen adsorption energy as a function of the coordination of the active sites are typically small (although systematic)[29].

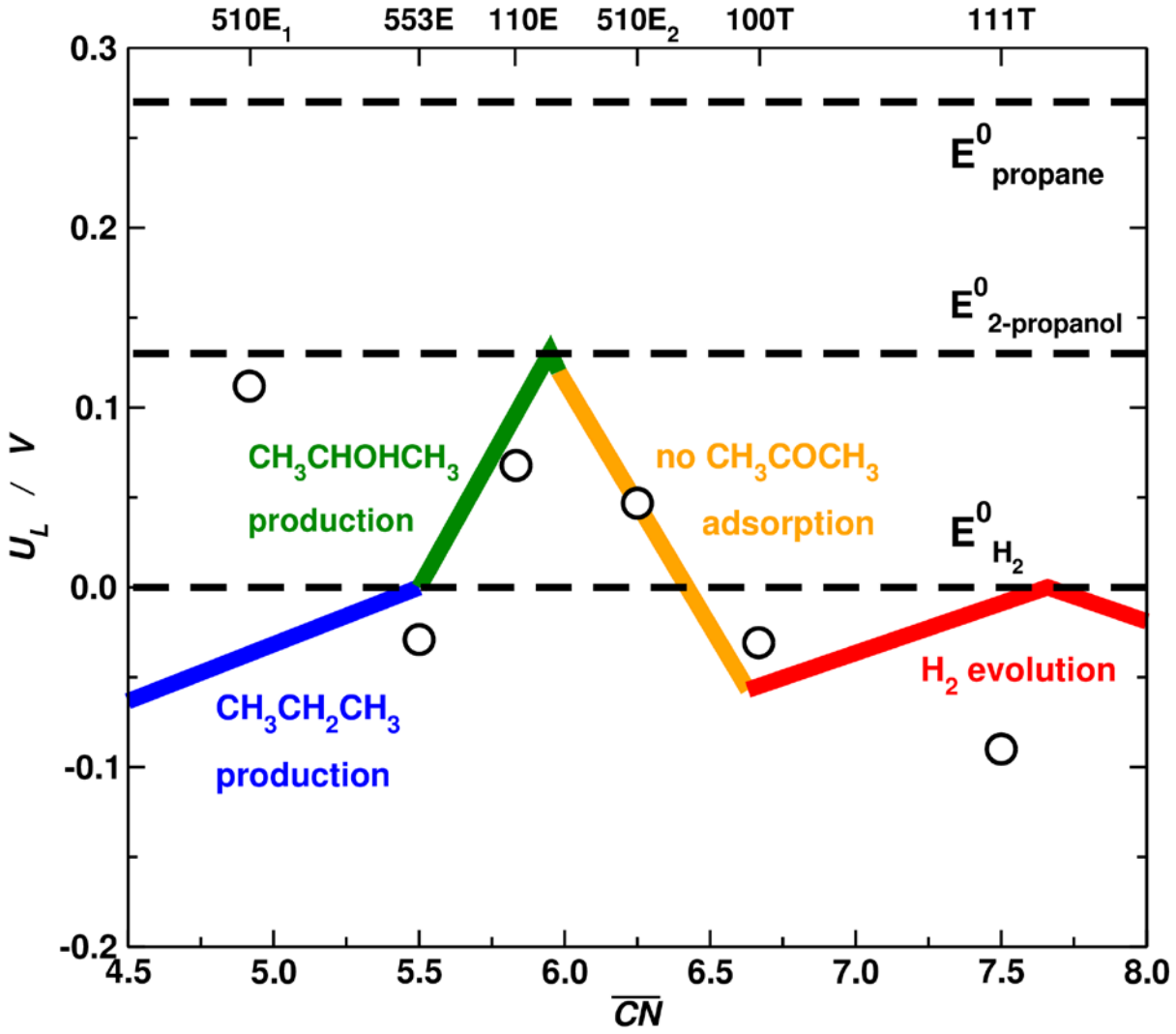

Figure 7. Structure-sensitive selectivity map for acetone reduction to 2-propanol and propane. The top x-axis locates the six different Pt sites under study, see also Supplementary Figure 16. The most favorable onset potentials (U_L) are reported in each case. The most active sites are the steps on Pt(110) for 2-propanol production, and (110) steps at Pt(510) for propane production. Black dashed lines represent equilibrium potentials. White dots are calculated data points from the DFT simulations. The data for H_2 evolution (red line) come from ref.[29], the orange, green and blue lines come from Figure 6 and are linear regressions built from 6 data points in each case. See Supplementary Note 8 and Supplementary Figure 18 for further details.

Extension of the Results to Other Aliphatic Ketones

The results obtained for the electrocatalytic hydrogenation of acetone at platinum single crystals has been extended to butanone and 3-pentanone. In Supporting Note 10 Supplementary Figures 20 to 28 compare the CVs in an acetone containing electrolyte with those recorded in butanone and pentanone containing electrolytes. Essentially, the same trends as for acetone are observed: with increasing step density of Pt(111)-type electrodes, the activity increases (c.f. also Supplementary Figure 29). However, as the carbon chain becomes longer, ketone reduction is shifted to more negative potentials. While acetone reduction takes place in a well-defined peak, butanone reduction takes place in a shoulder, and 3-pentanone reduction is barely distinguishable from hydrogen evolution. This might reflect a better stabilization of the C-O bond by hyperconjugation with the σ-orbital of a C-C bond in butanone and 3-pentanone compared to by hyperconjugation with the σ-orbital of a C-H bond in acetone.

A further difference between acetone, butanone and 3-pentanone becomes evident from Supplementary Figure 20. From the reversibility of the sulfate spike at Pt(111) we inferred that acetone does not adsorb at this electrode. While the spike in the first negative going scan appears in the presence of butanone and 3-pentanone, it is lost in the subsequent positive going scan. In the presence of 3-pentanone the spike is shifted to more positive potentials and hydrogen adsorption is shifted to more negative potentials both in the presence of butanone and pentanone. The altered adsorption energy for hydrogen and the change in the peak potential for sulfate adsorption indicate the adsorption of butanone and 3-pentanone, respectively. Since H-upd is not severely suppressed, the adsorption of butanone and 3-pentanone is weak and might be the result of enhanced van der Waals interactions due to the longer carbon chains.

From the CVs in Supplementary Figures 26 to 28 (c.f. also Supplementary Figure 30) it is less obvious that the reduction of butanone and 3-pentanone takes place at the steps of Pt(100)-type electrodes. However, this is evident from the OLEMS results in displayed in Supplementary Figure 31

and discussed in Supplementary Note 11. As in Figure 3, steps from 0.85 V into the potential region of butanone reduction have been conducted and in parallel the mass spectrometric response has been measured. The ionic current measured for mass 43 indicates the formation of butane, which is most prominent at Pt(510). Comparatively small amounts of butane are formed at pristine Pt(100). Hence, the reduction of higher aliphatic ketones proceeds at the steps of Pt(100)-type surfaces as well. In addition, no formation of butane is observed at Pt(553). Therefore, it can be concluded that higher ketones are also reduced to the corresponding alcohol at stepped Pt(111)-type electrodes.

DISCUSSION

Figures 1 and 2 show that acetone reduction does not proceed at the (111) and (100) basal planes of platinum. The activity of the platinum electrodes, thus, depends on the presence of steps. The DFT calculations (Figures 6 and 7) show that the interaction of acetone with Pt(111) and Pt(100) is energetically unfavorable due to the high coordination number of its surface atoms. Based on our experimental results, it was difficult to assess whether acetone reduction at stepped Pt(100) electrodes proceeds at (100) terraces and/or step sites. Figure 7 shows that the inactivity for acetone reduction is inherent to the (100) terraces and not caused by the poisoning reaction that occurs at it. Hence, acetone reduction takes place at the step sites of both Pt[(n-1)(111)x(110)] and Pt[(n+1)(100)x(110)] electrodes. However, experiments suggest that the poisoning of the electrode occurs due to a reaction taking place at (100) terraces. This poisoning reaction was not subjected to detailed investigation in this work as our emphasis was on the selectivity of the hydrogenation reaction, but it is observed that this reaction leads to the accumulation of incomplete oxidation products at Pt(100)-type electrodes, which ultimately results in the full deactivation of the catalyst (c.f. Supplementary Figure 9B). Furthermore, the poison can be removed oxidatively.

OLEMS (Figure 3) and FTIR (Figure 4) results show that the nature of the steps has a significant influence on product distribution. Acetone is reduced predominantly to 2-propanol at the steps of Pt[(n-1)(111)x(110)], while propane is formed at the step sites of Pt[(n+1)(100)x(110)]. The

selectivity map in Figure 7 explains that the different products are due to the dissimilar stabilization of reaction intermediates, which is a function of the coordination number of the active sites. The selectivity-determining intermediate is $*CH_3COHCH_3$ and the competing reactions are its hydrogenation and the cleavage of its C-O bond. Note in passing that once 2-propanol is desorbed from the surface, it neither adsorbs again nor undergoes further reduction according to both experiments and calculations. In other words, 2-propanol is not an intermediate of propane evolution from acetone, according to our observations.

In a previous paper, we suggested that the $*CH_3COHCH_3$ intermediate does not form from the keto tautomer[30]. Instead, acetone adsorbs either as propenol (its enol tautomer) or as protonated acetone from the solution. We have assessed the effect of propenol as prime reactant on our conclusions for Pt(510) and Pt(553) and the results are shown in Supplementary Figure 17. The onset potentials are nearly the same and so are the most favorable reaction pathways, which bifurcate on $*CH_3COHCH_3$ and differ only in the reactant. This gives confidence in the robustness of the computational results and substantiates the findings in Figures 5-7. In conclusion we have investigated the electrochemical hydrogenation of aliphatic ketones at platinum single crystal electrodes, with emphasis on acetone. The selectivity of the reaction displays a remarkable structural sensitivity: while no reaction proceeds at Pt(111) terraces, a reaction that ultimately leads to the electrode poisoning proceeds at Pt(100). In contrast, the actual hydrogenation on stepped surfaces happens at (110) steps, yielding different products: while aliphatic ketones are reduced to the corresponding alcohol at Pt(111)-type electrodes, Pt(100)-type electrodes catalyze hydrogenolysis to produce the respective hydrocarbon.

With the help of DFT calculations, we built a structure-sensitive selectivity map which suggests that the inability of (111) and (100) terraces to molecularly bind acetone and the predominance of *H adsorption and H_2 evolution renders them inactive and corroborates the experimental observation that (110) steps are the active sites for acetone reduction. A semi-

quantitative rationale for estimating whether the main product of acetone reduction will be 2-propanol or propane, based on the coordination number of the surface active site, was also provided.

The combination of detailed experimental and computational work presented here therefore allows us to conclude that surfaces with high generalized coordination number (Pt(111) and Pt(100)) do not adsorb acetone and are therefore inactive for the reduction of the ketone. 2-propanol is formed at Pt(553) and Pt(110) electrodes that feature medium generalized coordination numbers, and propane production occurs only at surfaces that feature low generalized coordination numbers such as that of the Pt(510) electrode. Furthermore, computational modeling elucidates the mechanism of acetone reduction in which the pathways to the alcohol and the hydrocarbon separate before 2-propanol is formed. This explains the experimental finding that acetone can be reduced to both propane and 2-propanol, but that the reduction of 2-propanol to the hydrocarbon is not measurable at Pt(510) electrodes.

METHODS

Chemicals and Materials

The blank electrolyte was prepared from *MilliQ* water and H_2SO_4 (suprapure, *Merck*). The ketones used were acetone (HPLC-grade, *Sigma-Aldrich*), butanone (>99%, *Sigma-Aldrich*) and 3-pentanone (>99%, *Sigma-Aldrich*). All solutions were freed from oxygen by purging with argon (6.0, *Linde*). All potentials were measured versus a reversible hydrogen electrode (RHE) in contact with the blank electrolyte. A platinum wire was used as a counter electrode. Under acidic conditions, ketones are expected to undergo a condensation reaction[31]. To avoid both the accumulation of condensation products and the depletion of the ketone, the electrolyte was changed every hour. Cyclic voltammograms (CV) were recorded on either a PGSTAT 12 potentiostat (*Autolab*) or an Iviumstat potentiostat (*Ivium Technologies*).

Single Crystal Electrodes

Electrochemical experiments and OLEMS (OnLine Electrochemical Mass Spectrometry) experiments were conducted with bead-type single crystals purchased from Icryst. Prior to each experiment the surface of the crystal was prepared by flame annealing following the protocol established by Clavilier[32]. The used glassware was kept for at least 8 hours in acidic permanganate solution. Prior to use, the glassware was rinsed with acidic peroxide solution and boiled several times in *MilliQ* water.

In the this paper, we use Pt(111), Pt(15,15,14), Pt((554), Pt(553), Pt(331) and Pt(110) electrodes. These surfaces are derived from the (111) basal plane by introducing (110) steps. While the terrace size of the (111) electrode is in theory infinite, its length is reduced to 30 atoms in Pt(15,15,14), 10 atoms in Pt(554), 5 atoms in Pt(553) and 3 atoms in Pt(331). In principle, there are no (111) terraces in the (110) surface. The step density on these surfaces increases accordingly, defined as $\theta_{step} = 1/(n-2/3)$,[33] where n is the width of the terraces (in number of atoms). However, in reality a (1x2) reconstruction of Pt(110) is observed[34]. In the ideal (1x2) reconstructed Pt(110) surface, every second row of (110)-step sites is missing, which reduces the step density by half and introduces 2 atom long (111) terraces.

The other set of electrodes was Pt(100), Pt(10,1,0) and Pt(510). These electrodes are derived from the (100) basal plane. In theory, the terrace width of Pt(100) is infinite. By introducing (110) steps the terrace width of the Pt(10,1,0) electrode is reduced to 10 atoms and that of the Pt(510) electrode to 5 atoms.

Online Electrochemical Mass Spectrometry

Online mass spectra were recorded in the multiple-ion detection mode at the indicated potentials on a PrismaPlus mass spectrometer (*Pfeiffer Vacuum*). A vacuum better than 10^{-5} mbar throughout the experiment was achieved by a turbo molecular pump with a suction power of 60 l/s. A Teflon frit inserted into an KelF-tip, was used as an interface between electrolyte and vacuum of the mass spectrometer[35]. The surface area of the Teflon frit was 0.8 mm^2. Volatile compounds can diffuse through the frit and an attached capillary into the vacuum.

In this setup the intensity of the mass spectrometric response depends not only on the amount of products, but also on the exact geometry of the setup. That is, the placement of the tip with respect to the electrode will influence the efficiency with which products are collected. Unfortunately, this geometry is difficult to reproduce between two different experiments and the sensitivity of the setup might vary. In order to ensure comparability of OLEMS data obtained in two different setups one can observe the mass spectroscopic response for a product that has the same formation rate in both experiments. If in this case the same signal intensity is observed, the collection efficiency between both setups is the same for any product. Since hydrogen evolution proceeds with very similar formation rates at Pt(553) and Pt(510), we use the signal on the ionic current for mass 2 to ensure that the collection efficiency and, therefore, the sensitivity in both experimental setups is the same.

Although our OLEMS results have a qualitative rather than quantitative character, we chose the OLEMS technique to study acetone reduction because of its high sensitivity (quantities corresponding to a single monolayer can be detected[36]) and because of the possibility to work in online mode during cyclic voltammetry. In theory an offline approach would allow quantification of the results, but is unsuitable for the present case: an offline approach requires the accumulation of reduction products, which is not possible due to the rapid deactivation of the Pt(510).

In situ Fourier-Transform Infrared Spectroscopy

Fourier-transform infrared spectra (FTIRS) were recorded on a Vertex V80 (*Bruker*). The used FTIR cell was home-built and accommodated a prism made of calcium fluoride[37]. By pressing the electrode with a diameter of 1 cm on the prism, a thin gap between electrode and prism was achieved. All spectra were recorded with a resolution of 4 cm^{-1} and are the average over 200 scans. A background spectrum was recorded at 0.85 V vs. RHE. Next, a potential step to the indicated values was performed and another spectrum was recorded, from which the background spectrum was subtracted.

Computational Details

The DFT simulations were made with VASP[38] using the PBE functional[39] and the projector augmented-wave method[40] . The topmost two layers of the slabs and the adsorbates were relaxed in all directions, whereas the bottommost ones were fixed at the bulk equilibrium distances. We used a plane-wave cut-off of 450 eV, k_BT = 0.2 eV (extrapolating the total energies to 0 K), and the conjugate-gradient scheme until the maximal force was <0.05 eV/Å. Monkhorst-Pack meshes[41] of 6×6×1, 6×6×1, 6×4×1, 4×3×1, and 5×3×1 for Pt(111), Pt(100), Pt(110), Pt(510), and Pt(553), ensured convergence of the adsorption energies within 0.05 eV. The distance between repeated images in the vertical direction was >14 Å and dipole corrections were used. Isolated molecules were calculated in boxes of 15 Å × 15 Å × 15 Å using k_BT = 0.001 eV and the Γ-point.

The reaction energies were approximated as: $\Delta G \approx \Delta E_{DFT} + \Delta ZPE - T\Delta S + \Delta E_{solvation}$, where ΔE_{DFT} is the DFT-calculated reaction energy, ΔZPE is the zero-point energy change and TΔS is the entropy change at 298.15 K. ΔS includes all contributions for free molecules and only vibrational entropy for adsorbates. Proton-electron pairs were modelled with the computational hydrogen electrode[42]. Solvation was modelled as an external correction depending on the chemical nature of the adsorbates[43,44], see the specific values in Supplementary Table 1. The generalized coordination number ($\overline{CN}$) of a surface site "*i*" is calculated based on the conventional coordination numbers (*cn*) of its n_i nearest neighbors as [45 46]:

$$\overline{CN}_i = \sum_{j=1}^{n_i} \frac{cn_j}{cn_{\max}} \quad (0)$$

where $cn_{\max}$ would be the number of nearest neighbors of the site if in the bulk, i.e. 12 for a single atom. The sites under study are shown in Supplementary Figure 17. The construction of coordination-activity plots for various reactions can be found in the SI and elsewhere,[22,47,48] the data for H_2 evolution come from reference[29].

The coordinates of the reaction intermediates on Pt(110) and Pt(510) are given in Supplementary Data 1.

DATA AVAILABILITY

All data is available from the authors upon reasonable request.

ACKNOWLEDGEMENTS

This research received funding from the Netherlands Organization for Scientific Research (NWO) in the framework of the fund New Chemical Innovations (project: 731.015.204 ELECTROGAS) with financial support of Akzo Nobel Chemicals, Shell Global Solutions, Magneto Special Anodes (Evoqua Water Technologies) and Elson Technologies.

F.C.-V. thanks the Spanish MEC for a Ramón y Cajal research contract (RYC-2015-18996) and acknowledges financial support from the "Units of Excellence María de Maeztu" program through grant MDM-2017–0767. The use of supercomputing facilities at SURFsara was sponsored by NWO Physical Sciences, with financial support by NWO.

Author Contributions

CJB co-conducted the FTIR experiments and conducted the remaining experimental work (i.e. CV studies, OLEMS studies and SERS studies), co-conceived the concept of the presented work and co-wrote the manuscript. FCV conducted the theoretical modeling, co-conceived the concept of the presented work and co-wrote the manuscript. MCF co-conducted the FTIR experiments. MTMK co-conceived the concept of the presented work and co-wrote the manuscript.

Competing interests

The authors declare no competing interest.

REFERENCES

1. Brown, T.R. & Brown, R.C. What role for the bioeconomy in an electrified transportation sector? *Biofuels, Bioproducts and Biorefining* **11**, 363-372 (2017).
2. Imam, T. & Capareda, S. Characterization of bio-oil, syn-gas and bio-char from switchgrass pyrolysis at various temperatures. *Journal of Analytical and Applied Pyrolysis* **93**, 170-177 (2012).
3. Oasmaa, A., Elliott, D.C. & Korhonen, J. Acidity of Biomass Fast Pyrolysis Bio-oils. *Energy & Fuels* **24**, 6548-6554 (2010).
4. Abu Bakar, M.S. & Titiloye, J.O. Catalytic pyrolysis of rice husk for bio-oil production. *Journal of Analytical and Applied Pyrolysis* **103**, 362-368 (2013).
5. Villalba, M., del Pozo, M. & Calvo, E.J. Electrocatalytic hydrogenation of acetophenone and benzophenone using palladium electrodes. *Electrochimica Acta* **164**, 125-131 (2015).
6. Cantu, D.C. et al. A Combined Experimental and Theoretical Study on the Activity and Selectivity of the Electrocatalytic Hydrogenation of Aldehydes. *ACS Catalysis* **8**, 7645-7658 (2018).
7. Song, Y. et al. Hydrogenation of benzaldehyde via electrocatalysis and thermal catalysis on carbon-supported metals. *Journal of Catalysis* **359**, 68-75 (2018).
8. Kwon, Y., de Jong, E., Raoufmoghaddam, S. & Koper, M.T.M. Electrocatalytic Hydrogenation of 5-Hydroxymethylfurfural in the Absence and Presence of Glucose. *ChemSusChem* **6**, 1659-1667 (2013).
9. Kwon, Y., Birdja, Y.Y., Raoufmoghaddam, S. & Koper, M.T.M. Electrocatalytic Hydrogenation of 5-Hydroxymethylfurfural in Acidic Solution. *ChemSusChem* **8**, 1745-1751 (2015).
10. Chadderdon, X.H. et al. Mechanisms of Furfural Reduction on Metal Electrodes: Distinguishing Pathways for Selective Hydrogenation of Bioderived Oxygenates. *Journal of the American Chemical Society* **139**, 14120-14128 (2017).
11. Hazzazi, O.A. et al. Electrochemical studies of irreversibly adsorbed ethyl pyruvate on Pt{h k l} and epitaxial Pd/Pt{h k l} adlayers. *Journal of Electroanalytical Chemistry* **640**, 8-16 (2010).
12. Rees, N.V. et al. In Situ Surface-Enhanced Raman Spectroscopic Studies and Electrochemical Reduction of α-Ketoesters and Self Condensation Products at Platinum Surfaces. *The Journal of Physical Chemistry C* **115**, 1163-1170 (2011).
13. Orito, Y., Imai, S. & Niwa, S. Asymmetric Hydrogenation of Methyl Pyruvate Using Pt-C Catalyst Modified with Cinchonidine. *NIPPON KAGAKU KAISHI* **1979**, 1118-1120 (1979).
14. Baltruschat, H. & Ernst, S. Molecular Adsorbates at Single-Crystal Platinum-Group Metals and Bimetallic Surfaces. *ChemPhysChem* **12**, 56-69 (2011).
15. Kita, H., Saito, K. & Katayama, A. ELECTROREDUCTION OF ACETONE ON PLATINUM IN SULFURIC ACID SOLUTION AND CATALYTIC ACTION OF PLATINUM AND MERCURY ELECTRODES. *Journal of the Research Institute for Catalysis* **25**, 45 - 62 (1977).
16. Bänsch, B., Härtung, T., Baltruschat, H. & Heitbaum, J. Reduction and oxidation of adsorbed acetone at platinum electrodes studied by DEMS. *Journal of Electroanalytical Chemistry and Interfacial Electrochemistry* **259**, 207-215 (1989).
17. de Hemptinne, X. & Schunck, K. Electrochemical reduction of acetone. Electrocatalytic activity of platinized platinum. *Transactions of the Faraday Society* **65**, 591-597 (1969).
18. Horányi, G. On the adsorption of organic compounds on platinized platinum electrodes. *Journal of Electroanalytical Chemistry and Interfacial Electrochemistry* **51**, 163-178 (1974).
19. Horányi, G. Electrocatalytic reductive splitting of C□O and C□OH bonds at platinum electrodes. *Electrochimica Acta* **31**, 1095-1103 (1986).
20. Calle-Vallejo, F. & Bandarenka, A.S. Enabling Generalized Coordination Numbers to Describe Strain Effects. *ChemSusChem* **11**, 1824-1828 (2018).

21. Löffler, T., Bussar, R., Xiao, X., Ernst, S. & Baltruschat, H. The adsorption of ethene on vicinally stepped electrode surfaces and the effect of temperature. *Journal of Electroanalytical Chemistry* **629**, 1-14 (2009).
22. Calle-Vallejo, F. et al. Why conclusions from platinum model surfaces do not necessarily lead to enhanced nanoparticle catalysts for the oxygen reduction reaction. *Chemical Science* **8**, 2283-2289 (2017).
23. Iwasita, T. & Pastor, E. A dems and FTir spectroscopic investigation of adsorbed ethanol on polycrystalline platinum. *Electrochimica Acta* **39**, 531-537 (1994).
24. Zaki, M.I., Hasan, M.A. & Pasupulety, L. In Situ FTIR Spectroscopic Study of 2-Propanol Adsorptive and Catalytic Interactions on Metal-Modified Aluminas. *Langmuir* **17**, 4025-4034 (2001).
25. McMurry, H.L. & Thornton, V. The Infrared Spectra of Propane and Its Symmetrical Deuterium Substituted Analogs. *The Journal of Chemical Physics* **19**, 1014 - 1018 (1951).
26. Dellepiane, G. & Overend, J. Vibrational spectra and assignment of acetone, ααα acetone-d3 and acetone-d6. *Spectrochimica Acta* **22**, 593-614 (1966).
27. Avery, N.R. EELS identification of the adsorbed species from acetone adsorption on Pt(111). *Surface Science* **125**, 771-786 (1983).
28. Koper, M.T.M. Thermodynamic theory of multi-electron transfer reactions: Implications for electrocatalysis. *Journal of Electroanalytical Chemistry* **660**, 254-260 (2011).
29. Pohl, M.D., Watzele, S., Calle-Vallejo, F. & Bandarenka, A.S. Nature of Highly Active Electrocatalytic Sites for the Hydrogen Evolution Reaction at Pt Electrodes in Acidic Media. *ACS Omega* **2**, 8141-8147 (2017).
30. Bondue, C.J. & Koper, M.T.M. A mechanistic investigation on the electrocatalytic reduction of aliphatic ketones at platinum. *Journal of Catalysis* **369**, 302-311 (2019).
31. Nielsen, A.T. & Houlihan, W.J. The Aldol Condensation. in *Organic Reactions* (John Wiley & Sons, Inc., 2004).
32. Clavilier, J., Armand, D., Sun, S.G. & Petit, M. Electrochemical adsorption behaviour of platinum stepped surfaces in sulphuric acid solutions. *Journal of Electroanalytical Chemistry and Interfacial Electrochemistry* **205**, 267-277 (1986).
33. Clavilier, J., El Achi, K. & Rodes, A. In situ probing of step and terrace sites on Pt(S)-[n(111) × (111)] electrodes. *Chemical Physics* **141**, 1-14 (1990).
34. Michaelis, R. & Kolb, D.M. Stability and electrochemical properties of reconstructed Pt(110). *Journal of Electroanalytical Chemistry* **328**, 341-348 (1992).
35. Wonders, A.H., Housmans, T.H.M., Rosca, V. & Koper, M.T.M. On-line mass spectrometry system for measurements at single-crystal electrodes in hanging meniscus configuration. *Journal of Applied Electrochemistry* **36**, 1215-1221 (2006).
36. Grimaud, A. et al. Activating lattice oxygen redox reactions in metal oxides to catalyse oxygen evolution. *Nature Chemistry* **9**, 457 (2017).
37. Iwasita, T., Nart, F.C. & Vielstich, W. An FTIR Study of the Catalytic Activity of a 85:15 Pt:Ru Alloy for Methanol Oxidation. *Berichte der Bunsengesellschaft für physikalische Chemie* **94**, 1030-1034 (1990).
38. Kresse, G. & Furthmüller, J. Efficient iterative schemes for ab initio total-energy calculations using a plane-wave basis set. *Physical Review B* **54**, 11169-11186 (1996).
39. Perdew, J.P., Burke, K. & Ernzerhof, M. Generalized Gradient Approximation Made Simple. *Physical Review Letters* **77**, 3865-3868 (1996).
40. Kresse, G. & Joubert, D. From ultrasoft pseudopotentials to the projector augmented-wave method. *Physical Review B* **59**, 1758-1775 (1999).
41. Monkhorst, H.J. & Pack, J.D. Special points for Brillouin-zone integrations. *Physical Review B* **13**, 5188-5192 (1976).
42. Nørskov, J.K. et al. Origin of the Overpotential for Oxygen Reduction at a Fuel-Cell Cathode. *The Journal of Physical Chemistry B* **108**, 17886-17892 (2004).

43. Calle-Vallejo, F. & Koper, M.T.M. Theoretical Considerations on the Electroreduction of CO to C2 Species on Cu(100) Electrodes. *Angewandte Chemie International Edition* **52**, 7282-7285 (2013).
44. He, Z.-D., Hanselman, S., Chen, Y.-X., Koper, M.T.M. & Calle-Vallejo, F. Importance of Solvation for the Accurate Prediction of Oxygen Reduction Activities of Pt-Based Electrocatalysts. *The Journal of Physical Chemistry Letters* **8**, 2243-2246 (2017).
45. Calle-Vallejo, F., Martínez, J.I., García-Lastra, J.M., Sautet, P. & Loffreda, D. Fast Prediction of Adsorption Properties for Platinum Nanocatalysts with Generalized Coordination Numbers. *Angewandte Chemie International Edition* **53**, 8316-8319 (2014).
46. Calle-Vallejo, F., Sautet, P. & Loffreda, D. Understanding Adsorption-Induced Effects on Platinum Nanoparticles: An Energy-Decomposition Analysis. *The Journal of Physical Chemistry Letters* **5**, 3120-3124 (2014).
47. Calle-Vallejo, F. et al. Finding optimal surface sites on heterogeneous catalysts by counting nearest neighbors. *Science* **350**, 185-189 (2015).
48. Calle-Vallejo, F., Pohl, M.D. & Bandarenka, A.S. Quantitative Coordination–Activity Relations for the Design of Enhanced Pt Catalysts for CO Electro-oxidation. *ACS Catalysis* **7**, 4355-4359 (2017).